

Unlayered graphenes in red-giant starsmoke

Eric Mandell, Nathaniel Hunton, and P. Fraundorf*

*Department of Physics and Astronomy and Center for Molecular Electronics,
University of Missouri - StL, St. Louis, Missouri 63121*

Electron diffraction, imaging, and energy loss provide evidence for unlayered graphene sheets in the core of certain interstellar graphite onions (from the meteorite Murchison) whose isotopes indicate formation in the atmosphere of late-stage asymptotic giant branch stars (like those which nucleosynthesized much of the earth's carbon). The data are compared to structural models loosely associated with atom-by-atom, molecule-by-molecule, and dendritic-droplet solidification processes. In this context the observed density, diffraction peak-shapes, and edge-on sheet patterns, along with theoretical limits on time for growth in the presence of outgoing radiation pressure, suggest nucleation of hexagonal sheets from pentagons, perhaps from a supercooled melt. These results warrant a closer examination of specimen structure, the energetics of unlayered graphene nucleation, and processes such as jets in late star atmospheres.

I. INTRODUCTION

This paper elaborates on a connection between two forefront areas of scientific inquiry: (i) single-walled carbon nanostructure formation, and (ii) the laboratory study of astrophysical dust formed around stars other than our own. In the former context, our observations may be relevant specifically to recent work on nucleation processes for single-walled carbon nanotubes¹, as well as evidence for the formation of single-walled conical² and multi-walled tubular³ carbon structures from liquid carbon droplets.

In the latter context, dust particles initially formed in the neighborhood of other nucleosynthesis sources, incorporated without melting during the formation of our solar system into future carbonaceous meteorites, and finally extracted for study in laboratories on earth, are proving to be a useful source of information on various astrophysical objects and processes⁴. Along with diamond, silicon carbide, and spinel, condensed phases identified as presolar include several graphite-related particle types. In particular, micron-sized “high-density” and isotopically heavy (i.e. with $^{12}\text{C}/^{13}\text{C} < \text{solar} = 89$) graphite spheres from the Murchison meteorite⁵ have “carbon-black” or “graphite onion” *rims* characterized by the concentric arrangement of 0.34 nm graphite layers. A sizable fraction of these rims appear to have nucleated not on the inorganic grains that have been used to constrain condensation conditions^{6,7}, but on a spherical *core* comprised of a novel carbon phase^{6,8}. In addition to its relevance to our knowledge of carbon processing in general, this phase may provide insight into precipitation processes in the atmospheres of AGB stars with surface temperatures low compared to our sun⁹, into astrophysical observations of cool stellar outflows^{10,11,12}, and into the state of interstellar condensed carbon^{13,14,15}.

The carbonaceous core phase in these presolar onions is comprised of atom-thick “flakes” around 4 nm across, with graphite (hk0) ordering but with no sign of the 0.34 nm (002) graphite layering characteristic of graphite, amorphous carbon, and multiwall carbon nanotubes, i.e.

of most solid non-diamond carbon phases^{6,16}. Intersecting line pairs in high resolution TEM images suggest that the sheets themselves may be bent by the occurrence of single cyclopentane defects occurring in place of perhaps one of every 400 graphene hexagons⁸, as though a significant fraction of the carbon atoms are in wide cone-angle faceted carbon nanocones. How one might pack a high abundance of faceted nanocones into a dense solid, while suppressing graphitic layering, is a mystery for earth-based processing. The fact that it happens in red-giant atmospheres, most likely to a significant fraction of the carbon ejected into the interstellar medium, only deepens the relevance of the mystery.

At one extreme, the cores might form by addition of one carbon atom at a time, with layer defects added in randomly from time to time to lessen entropy loss during the condensation process^{17,18}. Alternatively, they might form by the “collisional agglomeration” of previously-formed planar PAHs^{19,20}. At the other extreme, the cores might form by the dendritic crystallization of liquid carbon rain-drops condensed around magnetohydrodynamic jets in carbon-rich stellar atmospheres, before ejection by radiation pressure into the interstellar medium. In any of these cases, nucleation of the unlayered sheets might occur on lower-coordination (e.g. pentagonal) defects, or conversely the growing sheets might be converted from two into three dimensional structures by defects randomly-generated in the growing sheets. Observations which bear on these questions are reported in separate papers. Here, we look at what structural models linked loosely to these processes have to say in context of such observational data.

II. MODELS

Other papers associated with this work will focus first on the experiments. Here we begin with a set of simple models, loosely connected to the formation processes mentioned above. The models will be illustrated (Fig. 1) by high resolution electron microscope images, to which

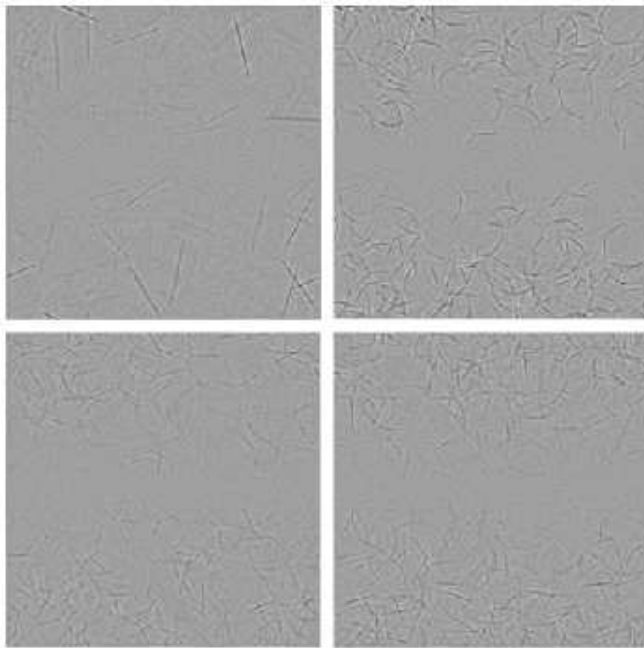


FIG. 1: Randomly-positioned graphene sheets (upper left), relaxed pentacones (upper right), faceted pentacones (lower left) and pentacones with two adjacent sheets parallel (lower right), seen in HRTEM image simulations of a specimen 22.5 nm square and 10 nm thick with a horizontal perforation.

they'll eventually be compared.

A. Agglomerated PAH's

One process suggested for the formation of these unlayered graphene cores has been the collisional aggregation of polycyclic aromatic hydrocarbon (PAH) molecules. They've been detected in astrophysical settings, and (as we confirm) they could explain the major features seen in electron diffraction patterns. Our first model for this is randomly-oriented graphene sheets like the 640 atom sheets illustrated in the upper left of Fig. 1.

The astrophysical difficulty associated with this, as a source of the graphene cores, is that incoming molecules are likely to have significant velocities (due to thermal, orbital, and radiation-pressure processes) relative to any prospective agglomerate. Even formation of large porous clusters seems difficult, given the expected kinetic energy of new arrivals. Formation of spherical particles whose density is comparable to that of graphite seems even less likely. Nonetheless, comparing the core material with randomly-oriented graphene sheets should be enlightening.

B. Corranulene Spirals

A second alternative is growth of unlayered graphenes from the vapor phase. PAH's form in space so this is certainly possible, provided one can prod the particles to grow in three dimensions rather than as sheets, without resorting to the van der Waals layering process (graphitization) so ubiquitous in non-diamond carbon on earth. The possibility of doing this with help from an occasional pentagon or heptagon in the sheet has already been proposed¹⁸. Although we are looking into atom-by-atom growth models as well, we simulate this alternative here with the random collection of relaxed (circular cross-section) pentacones shown in the upper right of Figure 1. These pentacones are relaxed because we expect that in vacuo the energy preference for sheet flatness will force all carbon atoms to share some of the curvature, at least as sheet coherence widths approach the 4 nm values seen in these specimens.

If growth occurs atom-by-atom, it is likely nucleation limited and the center of the particle might show some special features (not yet reported). There is also the mystery about suppressed graphite layering. If we have difficulty suppressing this layering even in amorphous carbon on earth, can radiation or some other process in the star's atmosphere allow graphene sheets to grow edge-wise without allowing atoms to start new van der Waals layered sheets as well. Although the energetic difference between such sites makes this possible, no quantitative process (experimental or theoretical) has been demonstrated to suppress layering so far.

C. Dendritic Solidification

A third alternative is dendritic solidification of a liquid carbon drop. Advantages of this are that it explains observed densities²¹ and the spherical core shape. There is an astrophysical problem with the sticking coefficient of incoming atoms²² that may also be ameliorated if the target cluster is liquid. As mentioned above, even though liquid carbon cannot equilibrate at low pressure it has been implicated in the laboratory formation of both single walled nanohorns and carbon nanotubes in low-pressure non-equilibrium processes. The high energy of sheet-edge attachment and proximity of atoms in the liquid might easily explain why graphene layering is suppressed as well. We also expect growth of sheets in a melt (possibly from pentagonal nuclei) would result in faceted nanocones since interstitial carbon would leave no room to relax. Thus our model for this is simply the faceted pentacones shown in the lower part of Figure 1. On the lower left, you'll find symmetric faceted cones like those you might expect if the pentagon is the nucleus. If pentagons also arise spontaneously during growth, flat growth might be redirected into three (not four) additional directions resulting in the asymmetric nanocones shown on the lower right.

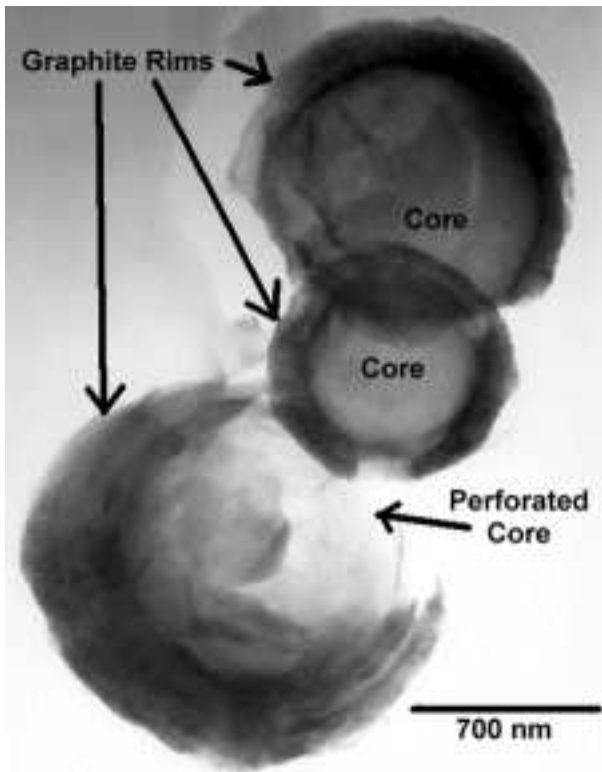


FIG. 2: Image of three onion slices, showing one with a torn core suitable for electron phase contrast study.

The disadvantage of this model is glaring. No one expects it. Since we have no direct experimental access to stellar atmospheres cool enough to condense carbon, this may be a case of finding the raindrop before we hear the storm, but its unexpectedness also means that more evidence for such processes will be needed to make it convincing. That’s why the focus of this paper has been on listening to what the specimens have to say.

III. EXPERIMENTAL

Figure 2 is an image of several graphite onions with an unlayered graphene core. They were from the Murchison meteorite graphite separate KFC1 (2.15-2.20 g/cm³), whose preparation has been described in detail by Amari et al.²³. The onions were microtomed to a thickness of 70 nm, and deposited onto 3mm copper grids with a holey carbon support film, by Bernatowicz et al.⁶. Specimens were examined in a 300 kV Philips EM430ST TEM with point resolution near 0.2nm.

Cleanly-sectioned cores large enough to minimize “spillover diffraction” from surrounding rims were the primary target for selected area diffraction measurements (c.f. Fig 2) on a TEM specimen designated KFC1A:E. Electron energy loss density measurements, and energy filtered maps, were taken on similar specimens. On the

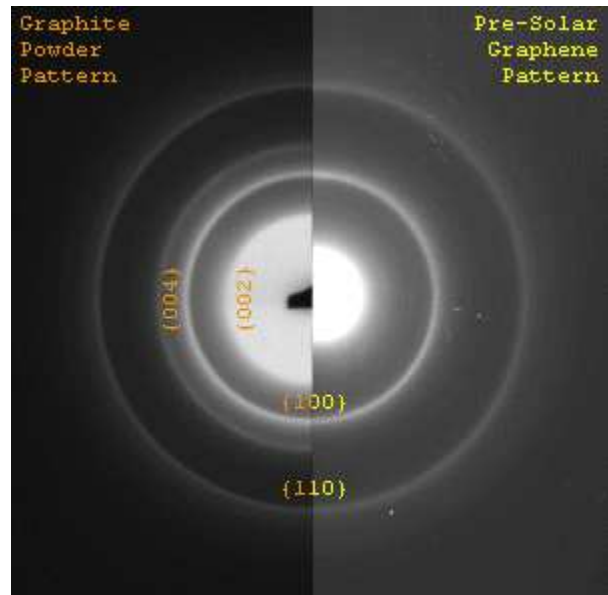


FIG. 3: Experimental diffraction pattern of polycrystalline graphite (left) and presolar unlayered graphene (right). Note the absence of all except (hk0) spacings in the latter, as well as the high frequency tails on each ring.

other hand, electron phase contrast (HRTEM) images focused instead on onions whose cores were torn during the sectioning, and positioned over a hole in the supporting carbon film. Image simulations were done using the strong phase object approximation. Further details of the data acquisition strategy are discussed elsewhere.

IV. DIFFRACTION DATA

Figure 3 compares the diffraction pattern of an onion core (right half) to that from graphitized carbon. The (hk0) peaks in both have “high frequency halos”, in the latter case because the carbon layers have graphitic onion morphology which makes it impossible for adjacent graphene sheets to retain coherence from layer to layer. Figure 4 shows one azimuthally-averaged “electron powder diffraction profile” from an onion core on a log-intensity scale. As you can see, all graphite reflections except for the six expected graphene (hk0) spacings are systematically absent from the patterns. This is true even for the graphite (002) spacing near $0.29[\text{\AA}^{-1}]$, easily detected in both diffraction and HRTEM imaging, and present in much terrestrial non-diamond carbon (including evaporated “amorphous” carbon support films, single-walled nanohorn²⁴ and nanotube collections because of the propensity of such tubes to align with van der Waals bonding between adjacent tube walls).

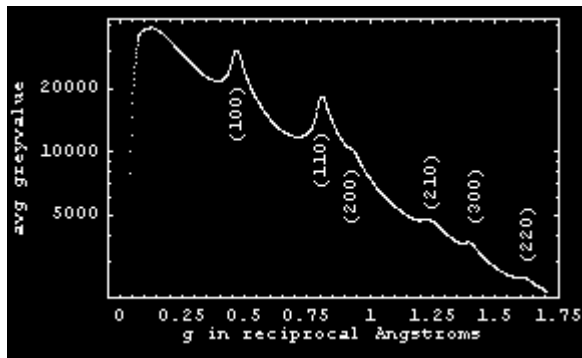


FIG. 4: Log plot of azimuthally-averaged greyvalue from a graphite-onion core, showing the presence only of “in-sheet” graphite (hk0) spacings out to 1.7 reciprocal Angstroms.

A. Flat sheet profiles

Azimuthally-averaged peak profiles like that in Fig. 5 allow one to see the asymmetric peak broadening (i.e. halos on the high-frequency side) characteristic of atom-thick crystals that continue to diffract even when highly foreshortened by tilt with respect to the incident beam. As a result, the product of peak full-width at half-maximum, and grain size is, is closer to $2 (\cong 1.84)^{25}$ than to values near 1 typical of equant 3D crystal shapes²⁶. This rule estimates mass-weighted average sheet sizes of 3.8 to 4[nm] for the (110) and (100) peaks of Figure 5, in agreement with sizes inferred from other onion core patterns by Bernatowicz et al.⁶. Further, comparable widths for the (110) and (100) reflections argues against systematic in-sheet anisotropy²⁷.

The Figure 5 analysis was done by adding random layer lattice profiles from Warren²⁵ for (100) and (110) rows of a single-size graphene sheet, plus a simple $a + b/g^2$ background, to azimuthally-averaged diffraction profiles whose intensity varied linearly with electron exposure. The consistency in peak asymmetry between experiment and theory (i.e. the common high-frequency tail), and the absence of graphite layering spacings like (002) in our experimental patterns, support the interpretation by Bernatowicz et al.⁶ that diffraction from this core material is indeed dominated by randomly-oriented atom-thick graphene sheets. The fit in Figure 5 is also shows that a single sheet-size alone does not explain details at the base of these peaks.

Similar fits were attempted using two different sheet sizes, or a log-normal distribution, with limited success. In other words, problems at the base of each peak (like the sharp cusp on the right side of the valley between both large peaks) remained. At this point, it began to seem that the feature responsible for broadening the base of the peak does not carry with it the asymmetry expected for sheets of atom-thick graphene, even though feature locations indicate graphene-like spacings.

Figure 6 fits a two-parameter model that combines graphene sheets of one size with broader gaussian peaks

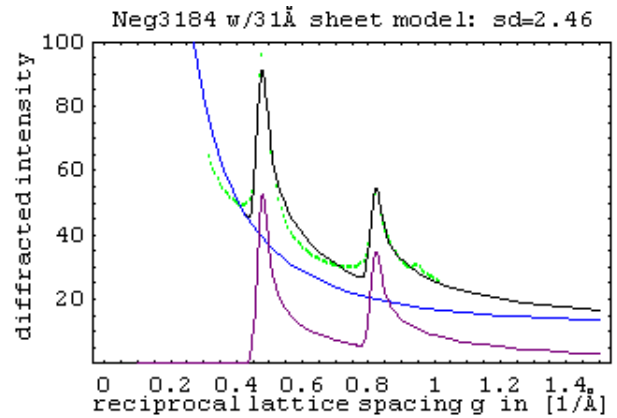


FIG. 5: Least-squares fit of core pattern 3184 (green) with a single-size sheet model (black) has the smallest standard deviation (2.46 greyvalue units) using 3.1[nm] sheets.

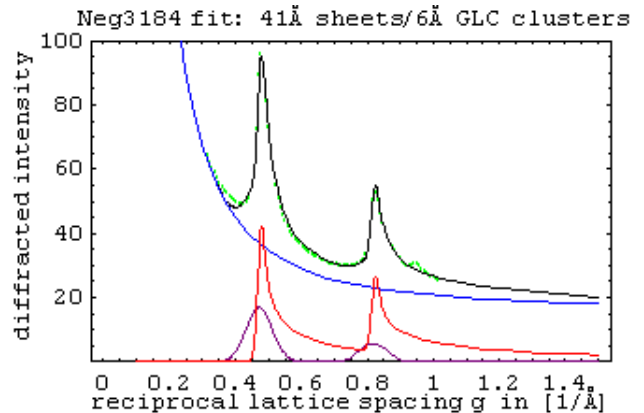


FIG. 6: Least-squares fit of core pattern 3184 (green) with a two-component mix (black) of graphene sheets and graphene-like carbon clusters has the smallest standard deviation (0.98 greyvalue units) for 4.1[nm] sheets and 0.6[nm] clusters.

at the graphene peak locations to one of several experimental spectra analyzed in this way. In each case the the systematic peak-shape problem was noticeably reduced, and the fit quality improved as well.

Instrumental broadening of peaks cannot explain the symmetric base-broadening component for two reasons. First, patterns from polycrystalline Al under the same illumination conditions limit the instrumental broadening full-width at half-maximum to the 0.01 reciprocal Angstrom range, much less than the 0.16 reciprocal Angstrom width of the symmetric residual. Secondly, the sharp leading edge of the asymmetric peaks of each core profile itself limits instrumental broadening to well under 0.05 reciprocal Angstroms.

Such peaks might also be due to “graphene-like carbon” clusters whose peaks do not show the asymmetry of atom-thick sheets. Since diamond also has essentially the same C-C bond lengths and hence first two reflections, one might also think of these as “diamond-

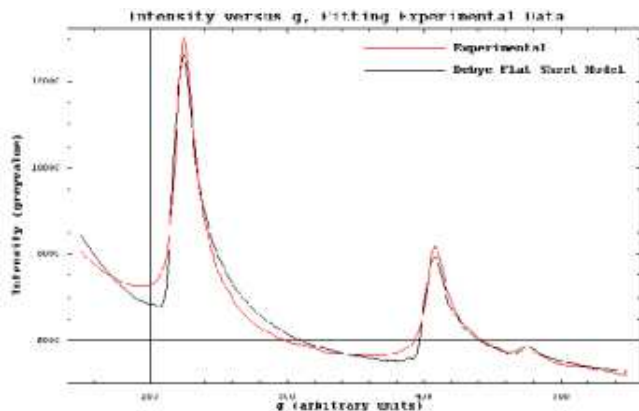


FIG. 7: Experimental diffraction data from a presolar core plotted with the best fit provided by a flat sheet Debye model.

like carbon” peaks although the lack of higher-order diamond reflections in Fig. 4 like those from pre-solar nanodiamonds²⁸, and plasmon energies seen in electron energy loss spectra⁶, limit the extent to which carbon- sp^3 ordering is actually present.

B. Correlated Sheet Profiles

To consider more complicated effects, profiles for unlayered graphene molecules were also calculated using the Debye scattering equation²⁹. Here, the diffraction intensity at each spatial frequency is computed by summing over all atoms in the structure. Since the Debye model works for any list of atom positions (given enough computer time), powder diffraction profiles for any list of atom positions may be computed from a sum over atom pairs. By creating a sheet-size fitting routine, we let the computer choose the best single-sheet size fit to experimental data. Figure 7 illustrates that the flat-sheet results are the same as those seen in the Warren model, where scattering on the low-frequency side and at the graphene periodicities remains unexplained.

A possible explanation for differences between the flat sheet model and experimental data are an effect which arises from the wide-range fringe visibility of atom-thick crystals³⁰, namely coherence effects from coordination between sheets. The Debye model (unlike Warren) lets us examine the effects of such sheet-sheet correlations. This can be seen in profile by comparing Debye models for one sheet of a faceted carbon nanocone with that for two adjacent facets, which make some non-zero angle with one another, where the profiles have been scaled for scattering by the same number of atoms. Figure 8 shows the profiles and their difference, where there is more scattering at the (110) peak due to the increased coherence width of that spacing across both facets, and a small satellite peak, corresponding to the preferential projection of this spacing across the facets, due to the angle between the two sheets. If we were to take many facets at different

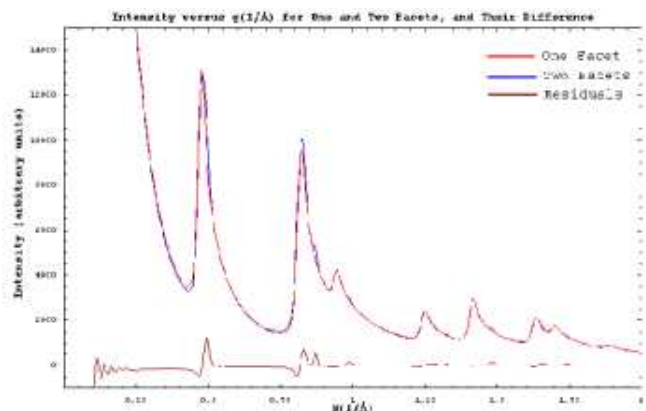


FIG. 8: A comparison of Debye diffraction patterns for one and two facets of the faceted nanocone. Observe the occurrence of a satellite peak on the (110) high frequency tail, due to the orientation of the facets.

angles, the satellite peaks would blur, yet we would see a small amount of extra scattering at the graphene periodicities. Early evidence from Debye work on collections of randomly-oriented multi-sheet structures (e.g. pentacones) suggests that coherence effects provide features similar to the differences seen between experimental data and single sheet models.

V. DENSITY MEASUREMENTS

Using a Leo-Zeiss 912 Energy Filtered TEM, we have obtained both brightfield TEM images, and zero-loss images of presolar graphite spherules. The brightfield images are typical unfiltered, phase contrast TEM images, while the zero-loss images are formed only with electrons which have undergone elastic scattering. The inelastic mean-free path is defined as the e-folding distance for zero-loss intensity with specimen thickness, and this in turn is proportional to projected potential and (for regions of similar composition) to mass densities in grams per cm^2 . Thus the ratio between inelastic mean free path at two locations (e.g. between the rim and core of a constant thickness slice) will to first order give us a ratio of mass densities per unit volume (ρ).

Serial EELS spectra on separate core and rim regions, obtained with a Gatan 607 series spectrometer, has suggested core densities around 0.65 relative to the graphitic rim ($\rho \simeq 2.2 \text{ g/cm}^3$). However, the microtome does not always slice uniformly across an onion. Therefore we also obtained thickness images using the log ratios of brightfield and elastic images taken with an energy-filtered TEM. Images were acquired with a CCD camera with no changes in illumination conditions between the two images, other than the energy filtering for the elastic image. Averaged intensity profiles are then taken over windowed sections of the resultant thickness map. Grey-value intensities for the core and rim can be compared,

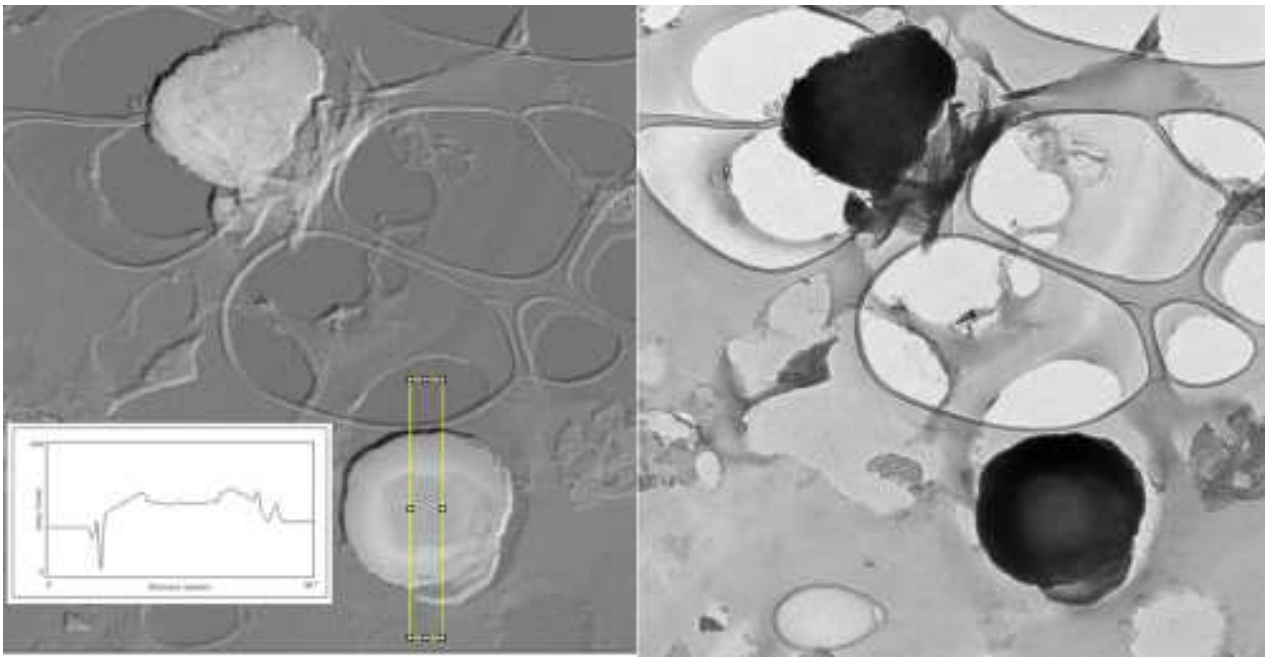


FIG. 9: A mean-free-path thickness map (a) calculated from a brightfield TEM image (b). The resulting greyvalue intensity profile (c) is shown for the windowed section in the thickness map. Intensities for the rim and core, relative to the hole, can be used to gauge density changes between the two regions.

relative to the greyvalue intensity of a hole in the image. Figure 9 shows the thickness map for two graphite spherules and the regular brightfield image for comparison. We concentrate on the spherule showing a strong core-rim structure, and calculate a greyvalue profile over the selected area shown. Comparing intensities for the rim and core, relative to the hole, intensity, we find core

to rim thickness ratios of 0.64. Thus the core material seems to have a density near 1.5 grams per cm^3 , i.e. lower than the 1.69 grams per cm^3 of buckminsterfullerene. This should be considered when comparing between the various proposed growth models, and further emphasizes the difference between presolar onion core and rim.

VI. HIGH RESOLUTION IMAGING

HRTEM work on core material⁸ has suggested the existence of coordinated graphene sheets, seen as end-connected linear features in images. Simulations (cf. Figure 1) show that edge-on graphene sheets, often intersecting at a point, indeed dominate the contrast. These simulations also show that relaxed nanocones (upper right) give noticeably stronger contrast fluctuations than do faceted cones or single sheets with the same number of atoms. Relaxed nanocones also give an appearance of curvature not reported in experimental images⁸, although more quantitative work is still needed to see if the experimental images indicate nanocone faceting, and perhaps even provide evidence for nucleation on pentagons.

Future work will be assisted by the availability of aberration-corrected microscopes. Figure 10 shows the center region of Figure 1 as it would look in a micro-

scope with twice the point resolution and a correspondingly better damping envelope. The biggest gain may come from an ability to see atom columns in the edge-on sheets, so that the coherence of intersecting segments can be investigated. Contrast fluctuations are also enhanced at higher resolution, so quantitative analysis of fluctuations should reveal new information as well.

VII. DISCUSSION

The data here confirms previous observations but shows that randomly-oriented flat sheets are not adequate to explain the diffraction data. It also indicates that the density of the core material is less than 2 grams per cm^3 , closer to that expected for frozen liquid carbon than for graphite, and shows how high resolution TEM imaging should be able to distinguish between sin-

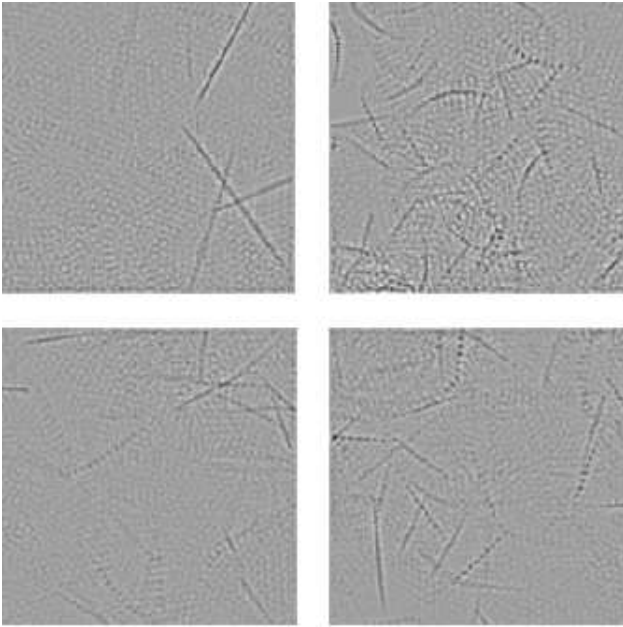


FIG. 10: Randomly-positioned graphene sheets (upper left), relaxed pentacones (upper right), faceted pentacones (lower left) and pentacones with two adjacent sheets parallel (lower right), seen in HRTEM image simulations at 1 Å resolution.

gle sheets, faceted pentacones, and relaxed pentacones. It also connects these structural alternatives to three different types of formation process: sheet agglomeration, atom-by-atom growth, or dendritic solidification of a liquid drop.

Other mysteries include the abrupt transition from unlayered graphene to normal onion growth (Fig. 2), the low “average” density of gas in grain-forming regions of red giant atmospheres which predicts too little time for growth prior to ejection by radiation pressure⁶, and the low sticking coefficient for carbon atoms incident onto

solid surfaces from the gas phase²². We are separately working to confirm interpretation of existing HRTEM data that suggests that “flat” graphene sheets³¹ connect pentagonal sheet defects, instead of the curved sheets one might expect if free-standing single-walled nanocones were allowed to relax before incorporation into the solid.

Might undercooled liquid-carbon droplets^{2,3} crystallize by dendritic growth of individual graphene sheets? The proximity of liquid atoms on both sides of a growing sheet could prevent both van der Waals layering, and sheet relaxation to accommodate strains caused by the occasional sheet defects which perturb sheet growth into new directions. Nucleation of this melt directly on pentagons might be consistent with recent studies of carbon nanotube energetics¹. Liquid carbon atoms left between “superstructure” sheets might have little choice but to form unsheetlike “gap-filling” structures on final solidification. The spherical core shape and density, a high sticking coefficient for incoming carbon atoms, and the abrupt transition to graphitic onion growth after solidification could all be explained nicely as well. Of course, if this unexpected conclusion pans out, the study of weather in cool stellar atmospheres may have to open up a new chapter on carbon rain.

Acknowledgments

Thanks to Tom Bernatowicz, Kevin Croat, and Roy Lewis for trusting us with specimens of unsliced and sliced graphite onions from Murchison for this work, and to Howard Berg for access to that energy-filtered TEM. This work has also benefited indirectly from support by the U.S. Department of Energy, the Missouri Research Board, as well as Monsanto and MEMC Electronic Materials Companies.

* Electronic address: pfraundorf@umsl.edu

¹ X. Fan, R. Buczko, A. A. Puretzky, D. B. Geohegan, J. Y. Howe, S. T. Pantelides, and S. J. Pennycook, *Phys. Rev. Lett.* **90**(14), 145501 (2003).

² D. Kasuya, M. Yudasaka, K. Takahashi, F. Kokai, and S. Iijima, *J. Phys. Chem B* **106**, 4947 (2002).

³ W. A. de Heer, P. Poncharal, C. Berger, J. Gezo, Z. Song, J. Bettini, and D. Ugarte, *Science* **307**, 907 (2005).

⁴ E. Zinner, *Ann. Rev. Earth Planet. Sci.* **26**, 147 (1998).

⁵ S. Amari, E. Zinner, and R. S. Lewis, *Meteoritics* **30**, 679 (1995).

⁶ T. Bernatowicz, R. Cowsik, P. C. Gibbons, K. Lodders, B. F. Jr., S. Amari, and R. S. Lewis, *Astrophysical Journal* **472**, 760 (1996).

⁷ T. K. Croat, T. Bernatowicz, S. Amari, S. Messenger, and F. J. Stadermann, *Geochim. et. Cosmochim. Acta* **67**, 4705 (2003).

⁸ P. Fraundorf and M. Wackenhut, *Ap. J. Lett.* **578**, L153

(2002).

⁹ J. M. Winters, T. L. Bertre, K. S. Jeong, C. Helling, and E. Sedlmayr, *Astron. Astrophys.* **361**, 641 (2000).

¹⁰ M. Frenklach and E. D. Feigelson, *Ap. J.* **341**, 372 (1989).

¹¹ I. Cherchneff, J. R. Barker, and A. G. G. M. Tielens, *Ap. J.* **401**, 269 (1992).

¹² D. Krueger, A. B. C. Patzer, and E. Sedlmayr, *Astron. Astrophys.* **313**, 891 (1996).

¹³ E. Sedlmayr, in *Molecules in the Stellar Environment*, edited by U. G. Jorgensen (Springer-Verlag, Berlin, 1994), no. 146 in IAU Colloquium, pp. 163–185.

¹⁴ M. Jura, in *Astrophysical implications of the laboratory study of presolar materials*, edited by T. J. Bernatowicz and E. Zinner (American Institute of Physics, Woodbury NY, 1997), no. 402 in AIP Conference Proceedings, pp. 379–390.

¹⁵ M. Chhowalla, H. Wang, N. Sano, K. B. K. Teo, S. B. Lee, and G. A. J. Amaratunga, *Phys. Rev. Lett.* **90**, 155504

- (2003).
- ¹⁶ T. J. Bernatowicz, P. C. Gibbons, S. Amari, and R. S. Lewis, in *Lunar and Planet. Sci. Conf. XXVI Abstracts* (Lunar and Planetary Institute, Houston TX, 1995).
 - ¹⁷ E. Sedlmayr and D. Krüger, in *Astrophysical implications of the laboratory study of presolar materials*, edited by T. J. Bernatowicz and E. Zinner (American Institute of Physics, Woodbury NY, 1997), no. 402 in AIP Conference Proceedings, pp. 425–450.
 - ¹⁸ H. W. Kroto and K. McKay, *Nature* **331**, 328 (1988).
 - ¹⁹ L. J. Allamandola, G. G. M. Tielens, and J. R. Barker, *Astrophysical Journal Supplement Series* **71**, 733 (1989).
 - ²⁰ T. J. Bernatowicz and R. Cowsik, in *Astrophysical implications of the laboratory study of presolar materials*, edited by T. J. Bernatowicz and E. Zinner (American Institute of Physics, Woodbury NY, 1997), no. 402 in AIP Conference Proceedings, pp. 451–474.
 - ²¹ L. M. Ghiringhelli, J. H. Los, E. J. Meijer, A. Fasolino, and D. Frenkel, *Phys. Rev. Lett.* **94**(14), 145701 (2005).
 - ²² B. P. Michael, J. A. Nuth, and L. U. Lilleht, *Astrophys. J.* **590**, 579 (2003).
 - ²³ S. Amari, R. S. Lewis, and E. Anders, *Geochim. Cosmochim. Acta* **58**, 459 (1994).
 - ²⁴ S. Bandow, F. Kokai, K. Takahashi, M. Yudasaka, L. C. Qin, and S. Iijima, *Chem. Phys. Lett.* **321**, 514 (2000).
 - ²⁵ B. E. Warren, *Phys. Rev.* **59**(9), 693 (1941).
 - ²⁶ A. L. Patterson, *Phys. Rev.* **56**, 978 (1939).
 - ²⁷ A. L. G. Rees and J. A. Spink, *Acta Cryst.* **3**, 316 (1950).
 - ²⁸ P. Fraundorf, G. Fraundorf, T. Bernatowicz, R. Lewis, and T. Ming, *Ultramicroscopy* **27**, 401 (1989).
 - ²⁹ B. E. Warren, *X-ray diffraction* (Addison-Wesley/Dover, New York, 1969/1990).
 - ³⁰ P. Fraundorf, W. Qin, P. Moeck, and E. Mandell, *Journal of Applied Physics* **98**, 114308 (2005).
 - ³¹ M. Liu and J. M. Cowley, *Ultramicroscopy* **53**, 333 (1994).